A&A 530, A117 (2011)
DOI: 10.1051/0004-6361/201015275

Astronomy & Astrophysics

XMM-Newton observations of the pre-polar HS0922+1333

J. Vogel, A. D. Schwope, and R. Schwarz

Leibniz-Institut für Astrophysik Potsdam (AIP), An der Sternwarte 16, 14482 Potsdam, Germany
e-mail: aschwope@aip.de

Received 24 June 2010 / Accepted 19 April 2011

ABSTRACT

We report on *XMM-Newton* and accompanying phase-resolved optical observations of HS0922+1333, one out of nine pre-polars. It shows X-ray and UV variability correlated with the visibility of the main accretion spot. The spectral X-ray properties reveal a low temperature thermal plasma of ∼1 keV with F_X more than one order of magnitude below the cyclotron flux. The UV data indicate a cool white dwarf with $T_{WD} < 8000$ K. We refine the ephemeris and determine a distance of 140 ± 50 pc. The derived location of the accretion spots yield a magnetic field axis laying nearly in the orbital plane. Optical spectroscopy uncovers a highly active secondary.

Key words. binaries: close – X-rays: binaries – novae – cataclysmic variables

1. Introduction

More than ten years ago two unusual magnetic binary systems were discovered in the Hamburg Quasar Survey, WX LMi (Reimers et al. 1999) and HS0922+1333 (Reimers & Hagen 2000). They were classified as magnetic cataclysmic variables (CVs) despite lacking some of the typical characteristics, strong atomic line emission and e.g. soft X-ray emission. Their spectra were just showing the two stellar components indicating low accretion states and one or two strong and well-isolated cyclotron emission lines. Further analysis revealed extreme low accretion rates $\dot{M} < 10^{-13}\ M_\odot\ \mathrm{yr}^{-1}$ for both objects, orders of magnitude below the normal accretion rate during a low state of a normal polar, a magnetic CV in synchronous rotation. In the following years seven more of those remarkable systems were discovered in the SDSS. They are now regarded as pre-polars, i.e. as the progenitors of polars, with the secondary not yet in Roche-lobe contact that are accreting from the stellar wind of the secondary (Schmidt et al. 2005; Webbink & Wickramasinghe 2005; Schwope et al. 2009).

Reimers & Hagen (2000) performed follow-up observations of HS0922+1333 with CAFOS at the 2.2 m telescope at Calar Alto Observatory. From the spectrum they derived a spectral type M3.5 of the secondary, a white dwarf temperature lower than 10 000 K, two accretion poles with a field strength of 66 and 81 MG respectively, with the second pole being extremely faint. The accretion rate was found to be less than $10^{-13}\ M_\odot\ \mathrm{yr}^{-1}$. Schwope et al. (2002) modeled the cyclotron component of the Reimers spectrum and obtained a field strength of $B = 67.3$ MG for the main accretion pole and a plasma temperature of 2 keV. Tovmassian & Zharikov (2007) performed spectroscopy covering a baseline of four years. They derived an accurate ephemeris with a period of 242.37 min.

Among the nine pre-polars known today four got already a dedicated observation in X-rays but only the two objects SDSS1553 (Szkody et al. 2004) and WX LMi (Vogel et al. 2007) have a proper X-ray detection, which allows for a detailed analysis. While all objects showed the same overall trend – a low temperature thermal plasma – for WX LMi a detailed phase resolved study of the X-ray emission was partly possible and revealed X-ray emission with likely contributions both from the corona of the secondary star and from the accretion region(s).

We observed HS0922+1333 with *XMM-Newton* primarily because of its short distance promising sufficient X-ray flux to analyse the accretion physics and the X-ray properties of the companion star. We also present new optical spectroscopy obtained in January 2006 when HS0922+1333 was observed as a backup target during a Calar Alto observing run.

Table 1. Observation log for optical spectroscopy with TWIN at the Calar Alto 3.5 m telescope and for the *XMM-Newton* observation.

Instrument	Filter	T_{exp}	Date	UT-start/end
TWIN		240 s	2006-01-22	01:28-06:19
IAC80	*V*	90 s	2008-11-04	03:27-06:34
PN	Thin	44.4 ks	2008-11-04	07:02-19:23
MOS1	Thin	46.0 ks	2008-11-04	06:40-19:27
MOS2	Thin	46.0 ks	2008-11-04	06:40-19:27
OM	*UVW1*	21.7 ks	2008-11-04	06:48-13:11
	UVM2	17.6 ks	2008-11-04	13:16-19:00

Notes. For the optical observations in the firsty two rows the third column lists the exposure times of individual images, otherwise the total exposure time. The orbital period of the binary is 14.5 ks.

2. Observations

2.1. Optical spectroscopy

HS0922+1333 was observed with the Calar Alto 3.5 m telescope on 2006, January 22 using the double-beam spectrograph TWIN. The gratings T05 and T06 for the blue and the red channel were used providing a dispersion of 36 Å/mm and resulting in a spectral coverage of 4105−5207 Å and 7633−8710 Å, respectively. Together with the 1.2″ slit used, these configurations yielded resolutions of 1.4 Å (blue) and 1.2 Å (red) *FWHM* as measured with Th/Ar arc-lamp spectra. Stability of the wavelength calibration has been ensured using the positions of notable night-sky lines and should be better than 3 km s^{-1}. Absolute flux calibration was performed using the standard stars Feige 24 and G191-B2B observed at the end of the night, while slit losses and extinction

variations have been approximately accounted for from spectra of a nearby star simultaneously kept in the slit. We obtained a series of 56 spectra with 240 s exposure time each, covering 1.2 orbits. However, clouds prevented uninterrupted observations, the phase interval 0.03−0.19 could not be covered (see Sect. 3.2 for phase convention). The observed wavelength range covers the third cyclotron harmonic for both accretion poles, the Hβ line and the sodium doublet.

2.2. Optical photometry

Quasi-simultaneous to the X-ray observation we performed optical photometry with the 80 cm reflector at the IAC from 03:27 to 6:34 UT on 2008, November 4 in V with an exposure time of 90 seconds covering nearly a complete orbit. The comparison star in the field of view used for reduction was SDSS J092503.28+131904.4 (with $V = 13\overset{\text{m}}{.}1$). The V band light curve is given in Fig. 5. The variability is due to beaming and visibility of the 3rd cyclotron harmonic and the spot.

We also observed HS0922+1333 in January and March 2006 with the 70 cm reflector of the AIP. All light curves show the same overall brightness during faint and bright phase among each other as well as compared to the IAC observation and are thus not shown here.

2.3. X-ray observation with XMM-Newton

The *XMM-Newton* observation was performed on 2008, November 11 for the duration of 45 ks between 06:39 and 19:31 UT, covering three complete orbits of the binary. The analysis of the X-ray data was performed with SAS version 8.0. The EPIC instruments were operated in full window imaging mode, the OM in fast mode using the *UVW1* and the *UVM2* filter. Owing to the low count rate the RGS gave no useful spectra at all. The data were reduced in the usual manner as described in the SAS user guide. The PN data were reduced using the SAS task *epreject* to extend the usable energy range down to 120 eV. This gave ~820 source photons in the PN and ~240 in each of the MOS cameras. All light curves were created using the SAS task *epiclccorr* to account for dead time, vignetting and PSF corrections. The OM data were reduced using the SAS task *omfchain*. The light curves are shown in Fig. 4 in original time sequence and in Fig. 5 folded over the orbital period. The X-ray and UV light curves are modulated with the visibility of the main accretion spot showing a bright phase from orbital phase 0.7 to 1.3, when the heated pole cap on the white dwarf and the accretion plasma can be seen, and a faint phase when the main accretion region is self-eclipsed by the white dwarf. Apart from this orbital modulation, the light curves for both bands show considerable irregularites. Around phase 6044.6 the *UVW1* light curve shows a steep increase during faint phase and one orbit later the X-ray light curve shows a flare-like but nevertheless long-lasting (~110 min) event.

3. Analysis

3.1. Orbital velocity of the secondary star

Orbital mean spectra obtained with the blue and red arms of the TWIN are reproduced in Fig. 1. We start the analysis with the red spectra which are dominated by photospheric emission from the companion star. The most prominent feature is the Na-doublet at 8183/8194 Å. This doublet displays pronounced wavelength shifts as a function of the orbital period. We measured the parameters of the NaI absorption lines in the individual spectra by

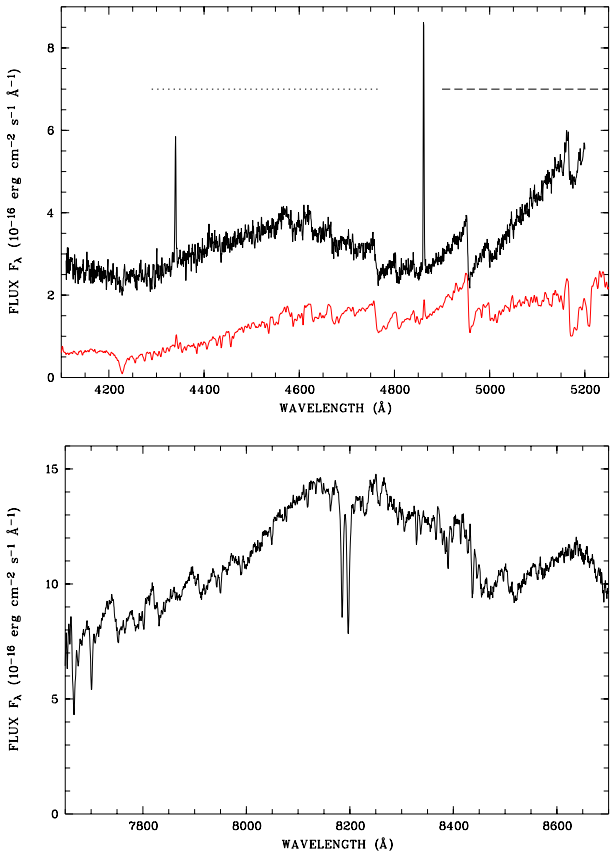

Fig. 1. Orbital mean spectra of HS0922+1333 obtained through blue and red arms of the TWIN, respectively. The blue spectrum also shows an arbitrarily scaled spectrum of an M3.5 dwarf. Horizontal lines above the spectrum mark the regions influenced by cyclotron harmonic emission, the 3rd harmonic in each case, from the secondary pole (dotted line) and the primary pole (dashed line), respectively.

Table 2. Radial velocity solutions for the NaI absorption and Hβ emission lines.

Line	γ [km s^{-1}]	K [km s^{-1}]
NaI8183/8194	21.7 ± 1.7	136.6 ± 2.3
Hβ	23.8 ± 4.6	114.3 ± 4.3

fitting double Gaussians with fixed separation, identical widths and fluxes. Those rather severe constraints were applied to cope with the low signal-to-noise ratio of some of the spectra.

The radial velocity curve was found to be fully compliant with a sinusoidal variation. The parameters of a circular orbit fit, $v_{\rm rad} = \gamma + K \sin 2\pi(t - t_0)$, are listed in Table 2, the data and the fit are shown in Fig. 2 (upper panel). The epoch of blue-to-red zero crossing is BJD = 2 453 757.6733 with an uncertainty of 40 s.

The only prominent emission line features in the blue spectra are the Hydrogen Hβ and Hγ lines. Hβ was about twice as intense as Hγ, we thus base our emission line radial velocity analysis only on the former line since Hγ could hardly be recognized in some of the individual spectra. The centroid wavelength of the Hβ emission lines was determined from Gaussian fits superposed on an assumed constant continuum. We found no indication for more complex line profiles. The lines are not resolved: the observed width of 2 Å (*FWHM*) is compatible with the instrumental resolution. Similarly to the NaI absorption lines, the Hβ line displays pronounced phase-dependent radial velocity shifts. The

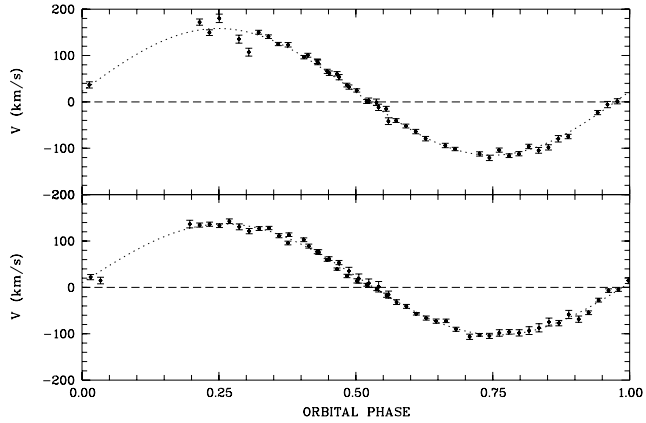

Fig. 2. Observed radial velocities and circular orbit fits for the NaI absorption lines (*top panel*) and the Hβ emission lines (*bottom panel*).

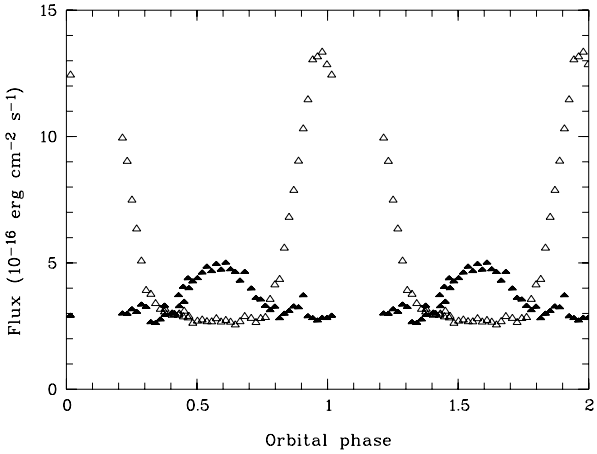

Fig. 3. Light curve for the 3rd cyclotron harmonic (5120−5200 Å) of the main accretion spot (open triangles) and for the 3rd harmonic (4440−4670 Å) of the secondary spot (filled triangles).

parameters of a circular orbit fit are also listed in Table 2, the data and the best-fitting sinusoid are displayed in the bottom panel of Fig. 2. The Hβ line also shows variability in the line flux by a factor of ∼1.8, with maximum emission around orbital phase 0.5 and minimum emission at phase 0.0.

Using the radial velocity semi-amplitude of 137 km s^{-1} for the sodium line as projected orbital velocity of the star we can estimate the inclination of the system. The secondary mass for a dM3.5 (Reimers & Hagen 2000) or dM4 (Tovmassian & Zharikov 2007) star is 0.35 $M_\odot$ or 0.32 $M_\odot$, respectively.

Assuming a mass of $M_{\rm WD} = 0.6\ M_\odot$ for the white dwarf the implied inclination is 37° for a 0.32 $M_\odot$ secondary and 36° for a secondary star with 0.35 $M_\odot$. For a more massive white dwarf, e.g. $M_{\rm WD} = 1\ M_\odot$ the inclination would be 56° or 53°, respectively.

At least the variable part of the Balmer emission lines is likely originating in a quasi-chromosphere of the secondary star. Its flux variability and lower radial velocity semi-amplitude compared to the sodium lines, indicate that such activity is concentrated at the hemisphere pointing towards the white dwarf.

3.2. Updated ephemeris

We use the epoch of phase zero of our spectroscopic observations of the NaI lines (see previous section) to update the spectroscopic ephemeris of Tovmassian & Zharikov (2007). The derived an ephemeris HJD = 2 452 308.336 + $E \times 0.168313$ using spectroscopic data covering a baseline of four years. The zero point of this ephemeris refers to the combined blue-to-red zero crossing of NaI absorption and Hα emission line radial velocity curves. Tovmassian & Zharikov (2007) did not publish an uncertainty of their zero epoch and we assume this to be 0.001 days. Using their period which they could determine with an uncertainty of 0.36 s we could determine the number of binary cycles between both epochs without cycle count ambiguity and further improve the accuracy of the period taking into account the estimated or measured 1σ uncertainties of both epochs for phase zero. We obtain the updated ephemeris

$$\mathrm{BJD\ (UT)} = 2\,453\,757.6733(5) + E \times 0.16831231(15) \qquad (1)$$

where the number in brackets represent the uncertainty in the last digits. This ephemeris is used throughout the paper.

3.3. Cyclotron component and spot location

The blue spectra obtained with the TWIN are covering the 3rd cyclotron harmonic originating from the main accretion spot only partly but that from the secondary spot fully. The identification of harmonic numbers follows Reimers & Hagen (2000) and Schwope et al. (2002). We use the blue wing, 5120−5200 Å, of the 3rd harmonic from the main pole to generate a light curve. The observation of the cyclotron spectrum from the main pole is further hampered by an incomplete phase coverage, the ingress into and the egress from the bright phase are nevertheless well covered. A light curve for the 3rd harmonic from the secondary region was constructed by integrating the spectra over the wavelength region 4440−4670 Å.

The light curves for both cyclotron harmonics observable in the blue spectral range are shown in Fig. 3. We used the center of maximum emission, determined via the *FWHM* of the cyclotron bright phase, as a marker for the spot location, obtaining phase 0.058 for the main spot and phase 0.58 for the secondary spot. This corresponds to an azimuth of $\Psi_1 \sim -20°$ and $\Psi_2 \sim 150°$, respectively. With the inclination derived in Sect. 3.1 the visibility of 0.69 and 0.43 phase units for the main and secondary spot constrains the colatitude to $\beta_1 \sim 70°$ for the main spot and $\beta_2 \sim 100°$ for the secondary spot (see e.g. Cropper 1988, for the definition of Ψ and β).

Since our new spectra do cover only a very small part of the cyclotron harmonic spectrum, we used the spectra presented by Reimers & Hagen (2000) (kindly made available to us by Dr. Hans Hagen) to measure the cyclotron flux of the main accretion spot. By comparing our new spectra and those of Reimers & Hagen (2000) in a spectral region and phase interval without cyclotron emission we find a factor 1.8 difference between both data sets, the newer spectra indicating an apparently brighter object. However, both observations were performed under non-favourable conditions and we regard the difference as due to calibration uncertainties and not due to the source's intrinsic variability. The magnitudes from SDSS, *ugriz* = 19.06, 18.14, 17.32, 15.88, and 14.99, respectively, are more compliant with the spectra from 2006. The integrated cyclotron flux in the observable second to fourth harmonics from the main accretion spot in the spectra of Reimers and Hagen corrected by a factor 1.8 is 3.1×10^{-12} erg cm^{-2} s^{-1}.

3.4. UV observations – the temperature and distance of the white dwarf

The UV observation were performed with the two filters *UVW1* and *UVM2*. Both filters cover more than one orbit each and both

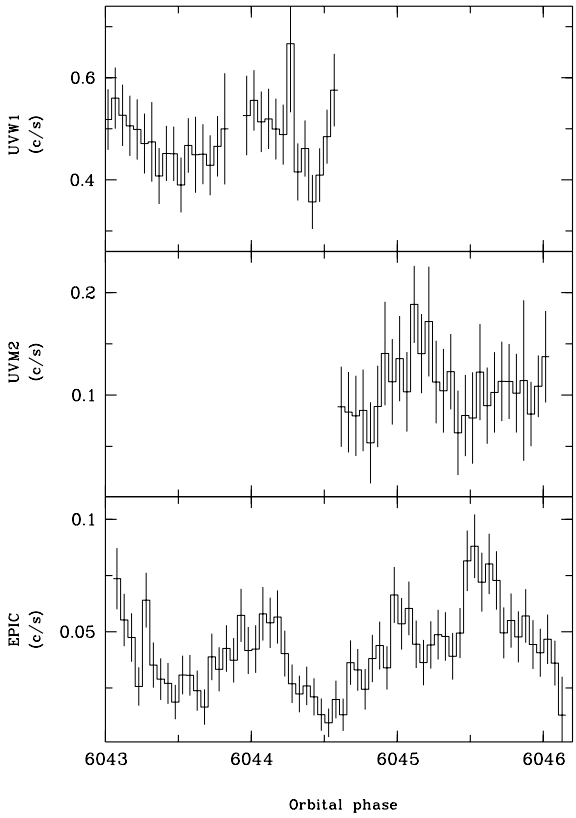

Fig. 4. The light curve for the OM in both used filters and the combined light curve for all three EPIC detectors phase-folded but in original time sequence. The optical *V* band observation (see Fig. 5) was performed one cycle before, from orbital phase 6042.16 to 6042.94.

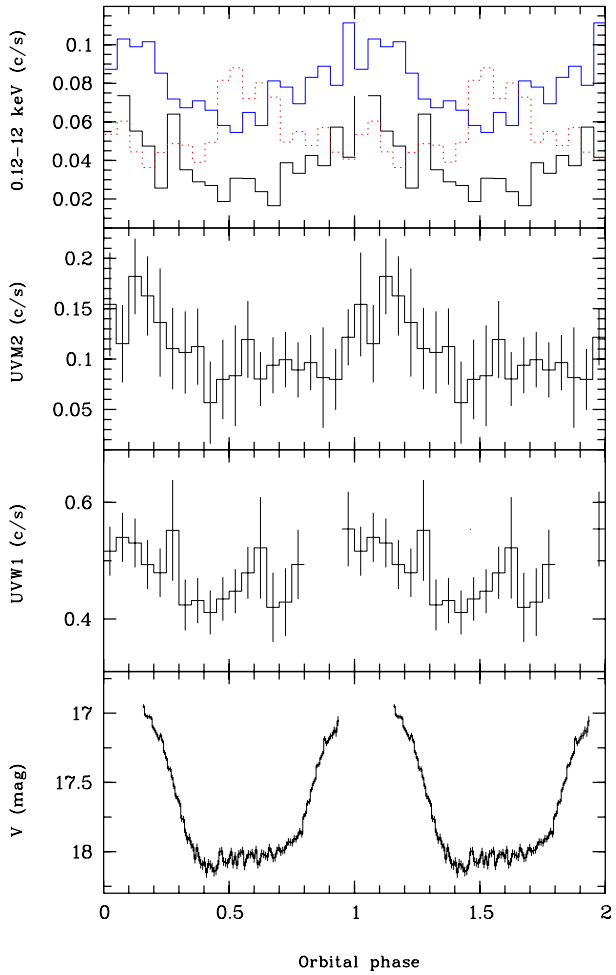

Fig. 5. Phase folded light curve of HS0922+1333 in X-rays (*top panel*), in the two UV filters (second and third panel from top), and in the optical *V* band (*bottom panel*). The light curves are plotted twice over orbital phase for clarity. For the X-ray light curve each orbit is plotted individually to exclude a deformation of the phase folded light curve due to the flare-like event in the third orbit. The individual X-ray light curves in the top panel are shifted to avoid mutual overlap. The first orbit in time is represented by the lower (black) solid line (shifted by 0.01 s^{-1}), the second orbit by the upper (blue) solid line (shifted by 0.045 s^{-1}) and the third orbit by the dashed line (not shifted). Error bars for the X-ray light curves are not given here for clearness but can be seen in the bottom panel of Fig. 4.

light curves are clearly modulated with the visibility of the main accretion spot (see Fig. 5). The faint phase of the phase folded *UVW1* light curve shows a steep increase at orbital phase 6044.6, which is not seen during the previous faint phase and whose origin is rather unclear.

Assuming that the UV light is completely dominated by the photosphere of the white dwarf the ratio between *UVW1* and *UVM2* light curve reflects directly the temperature of the photosphere and the heated pole cap. We folded white dwarf model spectra in the temperature range 8000−100 000 K (Gänsicke et al. 1995) through the response curves of the OM filters and detectors predicting a count rate ratio between the two filters as a function of the temperature. This procedure was verified by checking OM observations of the white dwarfs HZ4, GD50, and GD153 and found to be sufficiently accurate. The predicted count rate ratio increases with decreasing temperature and reaches a value of 4.5 for 8000 K. The count rate ratio for our observations remains roughly constant at ∼5 in the phase interval 0.3−0.8 (with a mean ratio of 5.1 ± 0.8), which implies a temperature below 8000 K. This is in agreement with the temperature estimate by Reimers & Hagen (2000), $T < 10\,000$ K. During orbital bright phase when the heated pole cap is in view the ratio decreases to a mean value of 3.8 ± 0.5 which implies a mean temperature of ∼9000 K with an uncertainty of ∼1000 K. Those temperature estimates may be biased through interstellar extinction. The column density of interstellar matter is non-negligible but otherwise not well constrained (see Sect. 3.5). To estimate the maximum effect on our derived temperatures we assume as maximum the total amount of galactic extinction in the direction of HS0922+1333, $N_{\rm H} = 3.5\times10^{20}$ cm^{-2}. The interstellar column density was transformed to $A_{\rm V}$ and to $A_{\rm X}$ (X being any band in the IR to UV spectral range) using the recipes given by Predehl & Schmitt (1995) and by Cardelli et al. (1989). The maximum correction factor for the filter ratio *UVW1*/*UVM2* thus becomes 20%, which transforms to a temperature increase of 1000 K for the two phase intervals defined above. The temperature shift may be much lower if the amount of interstellar matter is below the total galactic value, which appears likely given the rather short distance to the binary star.

The temperature estimate is supported by GALEX data, which gives a flux of 8.04 ± 1.98 μJ for the FUV band with an effective wavelength of 1516 Å and 35.98 ± 2.64 μJ for the NUV band (2267 Å). The time of observation corresponds to an orbital phase ∼0.17, i.e. the data are taken during orbital bright phase. GALEX data and XMM-OM are shown in Fig. 8 with a superimposed white dwarf model spectrum for a temperature of 8000 K.

Table 3. Spectral models and fit parameter for bright and faint phase interval.

Model	$n_{\rm H}$ [10^{20} cm^{-2}]	kT_1 [keV]	kT_2 [keV]	red. χ^2	NHP[a]	unabs. F^b erg cm^{-2} s^{-1}	unabs. $F^b_{\rm bol}$ erg cm^{-2} s^{-1}	L^c_X erg s^{-1}
bright phase:								
wabs*(MEKAL+MEKAL)	$3.7^{+3.1}_{-1.8}$	$0.31^{+0.04}_{-0.04}$	$0.98^{+0.14}_{-0.17}$	0.63	0.92	5.8	7.7	1.83
faint phase:								
wabs*(MEKAL+MEKAL)	$3.4^{+5.3}_{-2.8}$	$0.31^{+0.1}_{-0.1}$	$0.95^{+0.31}_{-0.29}$	0.95	0.51	2.6	3.3	0.77

Notes. Unabsorbed flux is given for the energy range 0.1−5 keV. [(a)] Null hypothesis probability; [(b)] in units of 10^{-14}; [(c)] in units of 10^{29} for a distance of 140 pc.

Using 8000 K as an upper limit to the temperature and assuming a mass of 0.6 $M_\odot$ the measured UV flux during the faint phase gives a distance of $D < 150$ pc. De-reddening could bring this number down to ∼125 pc. For a white dwarf with a mass as high as 0.8 $M_\odot$ the distance would be a further 25% shorter, i.e. about 95 pc. Without reddening and assuming a low mass white dwarf with 0.4 $M_\odot$ the distance could be as large as 190 pc.

HS0922+1333 has a measured K band magnitude of 12.53 (2MASS). The K band is centered at 2.15 μm while the cyclotron fundamental for a field strength of 66 and 81 MG lies at 1.6 and 1.3 μm, respectively. Thus the K band is expected to be free of cyclotron emission and to expose the M dwarf only. Using a surface brightness S_K of 4.2 for a spectral type M3.5 (Beuermann & Weichhold 1999) and a spectral type-radius relation for M dwarfs (Rebassa-Mansergas et al. 2007) the distance is ∼140 pc.

Reimers & Hagen (2000) estimated a distance of 190 pc from their optical spectrum using a template spectrum of spectral type dM3.5 for the secondary star. Their flux might be a factor 1.8 too low compared to our new spectra (see above), which would give a revised distance of ∼140 pc, consistent with our estimate based on the white dwarf and the K-band magnitude. We thus regard the distance likely in the range 95−190 pc with a current best estimate at ∼140 pc.

3.5. Phase-resolved X-ray spectroscopy

The mean X-ray spectrum contains ∼1300 photons in the three EPIC detectors and all the flux emerges below 5 keV. With the given number of photons we were able to perform a spectral analysis for the bright and faint phase separately. We created a bright phase spectrum for the orbital phase interval 0.8−1.2, where mainly the plasma component from the accretion spot contributes and a faint phase spectrum for the phase interval 0.3−0.7 covering just the first two observed faint phases. The third faint phase was excluded because of the flare-like event. All X-ray spectra were fitted simultaneously for all three detectors using *Xspec*[1]. The spectral parameter are summarised in Table 3.

For the bright phase spectrum, shown in Fig. 6 the data were binned to contain 20 photons per bin to allow for χ^2 minimization. To simulate the thermal plasma of the accretion region we initially chose the MEKAL model in *Xspec* absorbed by some amount of cold interstellar matter. A single plasma component ($\chi^2_\nu = 2.3$) could not reproduce the slope of the observed spectrum. Adding a second plasma component resulted in an acceptable fit with $\chi^2_\nu = 0.75$. The column density of interstellar matter determined by our fits of $N_{\rm H} = 3.1^{+3.2}_{-2} \times 10^{20}$ cm^{-2} is compatible with the average galactic column density of 3.5×10^{20} cm^{-2} given by the HEASARC *nH* tool.

[1] http://heasarc.gsfc.nasa.gov/docs/xanadu/xspec/

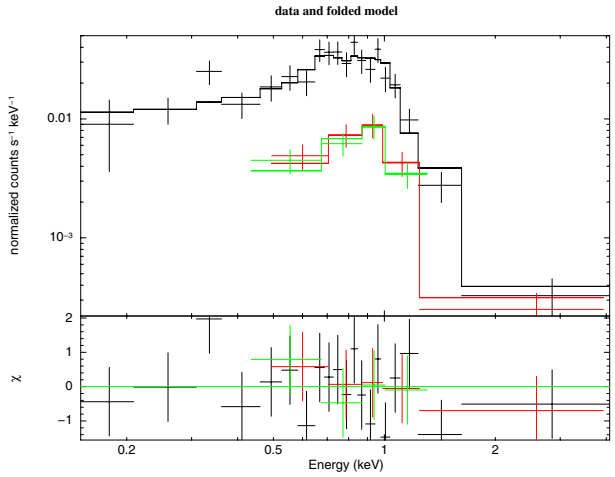

Fig. 6. Combined EPIC spectrum (all three detectors) for the orbital bright phase together with the absorbed two-temperature MEKAL model.

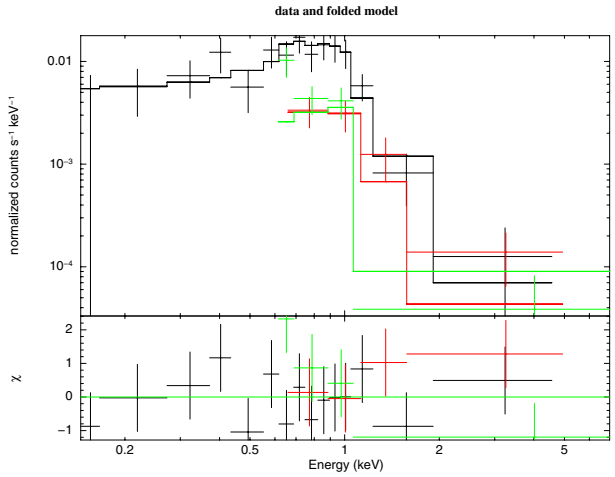

Fig. 7. Combined EPIC spectrum for the orbital faint phase together with the absorbed two-temperature MEKAL model.

The temperatures of the two thermal plasma components are significantly different. The temperature of the hotter component, ∼1 keV, is in rough agreement with that determined by optical cyclotron spectroscopy (Schwope et al. 2002) and thus likely is due to plasma emission from the main accretion pole. The second cooler component, ∼0.3 keV, could originate from the corona of the secondary star or a simple parameterization of the fact that the accretion plasma has a temperature structure.

The faint phase spectrum, shown in Fig. 7 with a binning of 10 photons per bin, contains only a little more than 200 photons. Similar to the bright phase spectrum an absorbed single

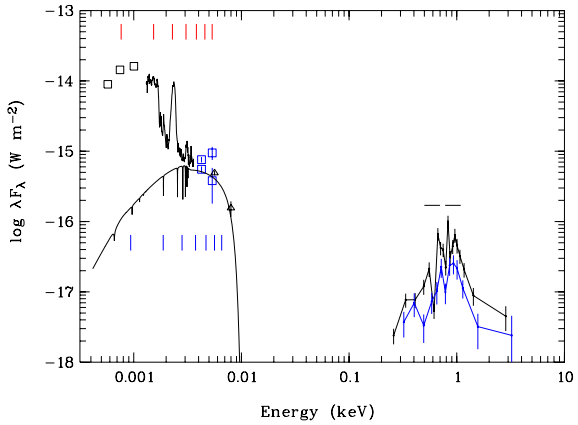

Fig. 8. Spectral energy distribution for HS0922+1333 showing 2MASS data (black squares), the optical spectrum (black line, Reimers & Hagen 2000), XMM-OM data for orbital bright and faint phase (blue squares), GALEX data (black triangles), and in the X-ray regime the EPIC-PN spectrum for orbital faint (blue line) and bright (black line) phase. The horizontal dashed line indicates the ROSAT upper limit, blue small vertical lines indicate the cyclotron harmonics for the secondary accretion spot (81 MG) and red vertical lines for the primary accretion spot (66 MG). Superimposed is a model atmosphere for a 0.6 $M_\odot$ white dwarf with a temperature of 8000 K and a distance of 140 pc.

plasma component was not sufficient to reproduce the slope of the spectrum, giving large residuals. An absorbed two-temperature model gave an acceptable fit ($\chi^2_\nu = 0.95$). Both the fit to the bright phase spectrum and the fit to the faint phase spectrum are consistent with each other. There is no significant change of spectral properties during the orbit. Also the hardness ratio created for the two bands 0.2−0.7/0.7−5.0 and 0.2−1.0/1.0−5.0 keV shows no significant change. We also performed a fit to the bright- and faint-phase spectra simultaneously with the column density and the plasma temperatures forced to be the same. Only the normalisation of the MEKAL models were allowed to be fitted independently. This gave a rather good fit with $\chi^2_\nu = 0.63$ and $kT_1 = 0.32^{+0.04}_{-0.04}$ keV, $kT_2 = 1.0^{+0.1}_{-0.1}$ keV and $n_{\rm H} = 3.6^{+2.4}_{-1.6}$ cm^{-2}. The normalisation for both MEKAL components varied by nearly the same factor with the visibility of the accretion region.

To inquire for spectral properties of the flare-like event we created a spectrum for the phase interval 6045.43 to 6045.73, containing ∼250 photons. A fit to the spectrum assuming a mono-energetic absorbed plasma did not reveal an acceptable fit, but as above the inclusion of a second plasma component gave an acceptable fit. Interestingly, both temperatures appear to be higher by a factor 2 compared to the bright and faint phase spectra, $kT_{\rm hot} = 2.0 \pm 0.7$ keV and $kT_{\rm cold} = 0.60 \pm 0.15$ keV, respectively.

We then created a rough light curve for the flare by averaging the light curve for the first two orbits and subtracting it from the third orbit to get an idea about the temporal behaviour of the flare. It shows a faster rise (∼30 min) than decrease (∼80 min) and covers a time span of ∼110 min. The flare has a possible origin as an accretion event on the white dwarf or it may be originating from the corona of the secondary star. We are lacking data with sufficient signal to noise to distinguish between both possibilities uniquely. Both, the active corona and the accretion process can both be described by a low temperature thermal plasma. The slow rise and the overall duration might argue against an origin from the secondary. Also the X-ray flare is not accompanied by any increase in the UV flux. Mitra-Kraev et al. (2005) derived a nearly linear correlation between X-ray and UV flux for flares on dMe stars. However, not every X-ray flare is also seen in the UV. The most obvious explanation as in the case of polars, an accretion event on the (secondary) accretion spot, also seems implausible since pre-polars are thought to accrete from the wind of the secondary, which makes a change in the accretion rate on this short time scale unlikely. One might think of an accretion mode where a reservoir of gas accumulates in the magnetosphere, reaches a critical density where its pressure overcomes the magnetic pressure and gets accreted via mass flow along magnetic field lines. If such a mode of accretion exists it would be different from accretion flares seen e.g. in UZ For Pandel & Córdova (2002) which was more likely due to anhanced mass transfer from the secondary star.

4. Summary and discussion

We analysed X-ray and UV observations of HS0922+1333 obtained with *XMM-Newton* together with optical spectroscopy obtained with the Calar Alto 3.5 m telescope. HS0922+1333 is one of three pre-polars providing sufficient X-ray flux for a detailed analysis. It shows a low-temperature accretion plasma with $kT \sim 1$ keV which is predominantly cooled by cyclotron radiation with $F_{\rm X}/F_{\rm cyc} < 0.05$. The plasma temperature (see Table 3) derived from the X-ray emission is in agreement with the temperature of ∼2 keV derived from the cyclotron modeling (Schwope et al. 2002). This confirms the prediction for the case of very low accretion rates which places HS0922+1333 in the bombardment accretion regime (Woelk & Beuermann 1996).

HS0922+1333 shows a very cool white dwarf with $T_{\rm WD} <$ 8000 K which restricts the accretion rate in the past to less than 10^{-11} $M_\odot$ yr^{-1}, at least for a time span shorter than the thermal timescale of the heated envelope, which is about 6×10^4 yr (Townsley & Bildsten 2003). The distance to HS0922+1333 is likely to be 140 ± 50 pc. The magnetic field shows an off-centred field configuration with the field axis nearly parallel to the orbital plane. This is also seen in the second well observed pre-polar WX LMi (Schwarz et al. 2001; Vogel et al. 2007) and rather unusual compared to polars. Quite some work has been spent to understand the synchronization of the white dwarf's spin with the orbit and the orientation of the main accreting pole (as a proxy for the magnetic axis) via the interaction of the large-scale magnetic fields and the presence of an accretion torque exerted by the accretion stream in polars (see e.g. King et al. 1990; Campbell 1997; Wu & Wickramasinghe 1993, and references to those papers). The stable phase relation between the azimuth of the main spot and the secondary star indicates that the white dwarf in HS0922+1333 is synchronized. King et al. (1990) conclude that a stable configuration in polars requires that the two dipoles involved must lie in the orbital plane and that the accretion flow in the vicinity of the white dwarf is controlled by higher magnetic multipoles. The measured orientation of the white dwarf's dipole axis in HS0922+1333 and WX LMi close to the orbital plane in the "clean" environment of a long-period pre-polar (weak accretion torque, braking via magnetized wind) might be regarded as support of their model.

The Hβ emission line, in phase with the NaI absorption line, is indicative of an active secondary. The radial velocity semi-amplitude of (114.3 ± 4.3 km s^{-1}) is somewhat smaller than for the Naı line. This is consistent with the variability of the Hβ line flux, showing stronger emission at superior conjunction of the secondary, and implies a non-uniform emission from the secondary. The fact that the Hβ emission is not centred on the

stellar disk, instead shifted towards the hemisphere facing the white dwarf is typically interpreted in terms of irradiation, but seems arguable in the case of a cold white dwarf and low accretion rates. Active stars also show X-ray activity. With the two accretion poles rotating alternatively into the field of view it is hard to disentangle accretion plasma and possible contribution of the secondary star in our X-ray spectra since corona and the accretion process can both be described by a low temperature thermal plasma. The cyclotron light curves show the minimum cyclotron contribution at phase ∼0.4, which coincides roughly with the X-ray minimum. Anyhow, using the lowest bin in our X-ray light curve at phase 6044.53 the upper limit for the X-ray contribution of the secondary is $F_X = 1.5 \times 10^{-14}$ erg cm^{-2} s^{-1} and thus $L_X = 3.5 \times 10^{28}$ erg s^{-1}. Together with the bolometric luminosity of 1.97×10^{32} erg s^{-1} for a M3.5 secondary star (Leggett et al. 1996) this gives $L_X/L_{bol} \sim 0.2 \times 10^{-3}$, which is comparable to the values observed within the X-ray saturated regime for rapidly rotating low mass stars (Pizzolato et al. 2003). Taking the possible contribution of the secondary star into account, the X-ray flux for the main accretion spot decreases to 6.2×10^{-14} erg cm^{-2} s^{-1}, which gives a huge excess of cyclotron cooling versus thermal X-ray radiation of $F_{cyc}/F_X > 50$.

HS0922+1333 fits in well in the sample of known pre-polars. It was the second of the group of nine objects. A more detailed disquisition of the evolutionary status of the pre-polars as a class can be found e.g. in Schmidt et al. (2007) or Schwope et al. (2009). The sample is still rather small and due to the intrinsic faintness of pre-polars not all properties can be determined for every system. But as a class they share the same characteristics. Compared to polars they all have accretion rates below 3×10^{-13} $M_\odot$ yr^{-1}, compatible with accretion from the wind of the secondary and a very cold white dwarf which makes a heating by accretion and thus an accretion rate as observed in polars very unlikely. They all show a low temperature accretion plasma with $kT \sim 1$ keV. The three systems which are never observed in X-rays (SDSS1031, SDSS1059 and SDSS1206) are unlikely to provide sufficient X-ray flux due to their large distance. Nevertheless the cyclotron properties imply a low plasma temperature of ∼1 keV (Schmidt et al. 2007; Schwope et al. 2009).

Acknowledgements. We thank Cristina Zurita and Esteban Currás for providing observing time and performing the observations at the IAC80 telescope. We also thank Klaus Reinsch for providing MONET observing time on short notice. We are grateful to Hans Hagen who provided the spectra of their original discovery paper.
We acknowledge helpful criticism by an anonymous referee.
J.V. was supported by the Deutsches Zentrum für Luft- und Raumfahrt (DLR) GmbH under contract No. FKZ 50 OR 0807.
This article is based on observations obtained with *XMM-Newton*, an ESA science mission with instruments and contributions directly funded by ESA Member States and NASA. This article also uses observations made with the IAC80 telescope operated on the island of Tenerife by the Instituto de Astrofisica de Canarais in the Spanish Observatorio del Teide and observations made with the NASA Galaxy Evolution Explorer (GALEX). GALEX is operated for NASA by the California Institute of Technology under NASA contract NAS5-98034.

References

Beuermann, K., & Weichhold, M. 1999, in Annapolis Workshop on Magnetic Cataclysmic Variables, ed. C. Hellier, & K. Mukai, ASP Conf. Ser., 157, 283
Campbell, C. G. 1997, Magnetohydrodynamics in Binary Stars, Astrophys. Space Sci. Lib., 216,
Cardelli, J. A., Clayton, G. C., & Mathis, J. S. 1989, ApJ, 345, 245
Cropper, M. 1988, MNRAS, 231, 597
Gänsicke, B. T., Beuermann, K., & de Martino, D. 1995, A&A, 303, 127
King, A. R., Whitehurst, R., & Frank, J. 1990, MNRAS, 244, 731
Leggett, S. K., Allard, F., Berriman, G., Dahn, C. C., & Hauschildt, P. H. 1996, ApJS, 104, 117
Mitra-Kraev, U., Harra, L. K., Güdel, M., et al. 2005, A&A, 431, 679
Pandel, D., & Córdova, F. A. 2002, MNRAS, 336, 1049
Pizzolato, N., Maggio, A., Micela, G., Sciortino, S., & Ventura, P. 2003, A&A, 397, 147
Predehl, P., & Schmitt, J. H. M. M. 1995, A&A, 293, 889
Rebassa-Mansergas, A., Gänsicke, B. T., Rodríguez-Gil, P., Schreiber, M. R., & Koester, D. 2007, MNRAS, 382, 1377
Reimers, D., & Hagen, H.-J. 2000, A&A, 358, L45
Reimers, D., Hagen, H.-J., & Hopp, U. 1999, A&A, 343, 157
Schmidt, G. D., Szkody, P., Vanlandingham, K. M., et al. 2005, ApJ, 630, 1037
Schmidt, G. D., Szkody, P., Henden, A., et al. 2007, ApJ, 654, 521
Schwarz, R., Schwope, A. D., & Staude, A. 2001, A&A, 374, 189
Schwope, A. D., Brunner, H., Hambaryan, V., & Schwarz, R. 2002, in The Physics of Cataclysmic Variables and Related Objects, ed. B. T. Gänsicke, K. Beuermann, & K. Reinsch, ASP Conf. Ser., 261, 102
Schwope, A. D., Nebot Gomez-Moran, A., Schreiber, M. R., & Gänsicke, B. T. 2009, A&A, 500, 867
Szkody, P., Homer, L., Chen, B., et al. 2004, AJ, 128, 2443
Tovmassian, G. H., & Zharikov, S. V. 2007, A&A, 468, 643
Townsley, D. M., & Bildsten, L. 2003, ApJ, 596, L227
Vogel, J., Schwope, A. D., & Gänsicke, B. T. 2007, A&A, 464, 647
Webbink, R. F., & Wickramasinghe, D. T. 2005, in The Astrophysics of Cataclysmic Variables and Related Objects, ed. J.-M. Hameury, & J.-P. Lasota, ASP Conf. Ser., 330, 137
Woelk, U., & Beuermann, K. 1996, A&A, 306, 232
Wu, K., & Wickramasinghe, D. T. 1993, MNRAS, 260, 141